The clock and wavefront model revisited

Philip J. Murray, Philip K. Maini, Ruth E. Baker

▶ **To cite this version:**

Philip J. Murray, Philip K. Maini, Ruth E. Baker. The clock and wavefront model revisited. Journal of Theoretical Biology, 2011, 283 (1), pp.227. 10.1016/j.jtbi.2011.05.004 . hal-00719493

HAL Id: hal-00719493
https://hal.science/hal-00719493

Submitted on 20 Jul 2012

HAL is a multi-disciplinary open access archive for the deposit and dissemination of scientific research documents, whether they are published or not. The documents may come from teaching and research institutions in France or abroad, or from public or private research centers.

L'archive ouverte pluridisciplinaire **HAL**, est destinée au dépôt et à la diffusion de documents scientifiques de niveau recherche, publiés ou non, émanant des établissements d'enseignement et de recherche français ou étrangers, des laboratoires publics ou privés.

Author's Accepted Manuscript

www.elsevier.com/locate/yjtbi

The clock and wavefront model revisited

Philip J. Murray, Philip K. Maini, Ruth E. Baker

PII: S0022-5193(11)00238-4
DOI: doi:10.1016/j.jtbi.2011.05.004
Reference: YJTBI6468

To appear in: *Journal of Theoretical Biology*

Received date: 2 October 2010
Revised date: 24 January 2011
Accepted date: 3 May 2011

Cite this article as: Philip J. Murray, Philip K. Maini and Ruth E. Baker, The clock and wavefront model revisited, *Journal of Theoretical Biology*, doi:10.1016/j.jtbi.2011.05.004

This is a PDF file of an unedited manuscript that has been accepted for publication. As a service to our customers we are providing this early version of the manuscript. The manuscript will undergo copyediting, typesetting, and review of the resulting galley proof before it is published in its final citable form. Please note that during the production process errors may be discovered which could affect the content, and all legal disclaimers that apply to the journal pertain.

ACCEPTED MANUSCRIPT

The clock and wavefront model revisited

Philip J. Murray[a,*], Philip K. Maini[a,b], Ruth E. Baker[a]

[a] *Centre for Mathematical Biology, Mathematical Institute, 24-29 St Giles, Oxford, OX1 3LB, UK*
[b] *Oxford Centre for Integrative Systems Biology, Department of Biochemistry, South Parks Rd, Oxford OX1 3QU, UK*

Abstract

The currently accepted interpretation of the clock and wavefront model of somitogenesis is that a posteriorly moving molecular gradient sequentially slows the rate of clock oscillations, resulting in a spatial readout of temporal oscillations. However, while molecular components of the clocks and wavefronts have now been identified in the pre-somitic mesoderm (PSM), there is not yet conclusive evidence demonstrating that the observed molecular wavefronts act to slow clock oscillations. Here we present an alternative formulation of the clock and wavefront model in which oscillator coupling, already known to play a key role in oscillator synchronisation, plays a fundamentally important role in the slowing of oscillations along the anterior-posterior (AP) axis. Our model has three parameters which can be determined, in a given species, by the measurement of three quantities: the clock period in the posterior PSM, somite length and the length of the PSM. A travelling wavefront, which slows oscillations along the AP axis, is an emergent feature of the model. Using the model we predict: (a) the distance between moving stripes of gene expression; (b) the number of moving stripes of gene expression and (c) the oscillator period profile along the AP axis. Predictions regarding the stripe data are verified using existing zebrafish data. We simulate a range of experimental perturbations and demonstrate how the model can be used to unambiguously define a reference frame along the AP axis. Comparing data from zebrafish, chick, mouse and snake, we demonstrate that (a) variation in patterning profiles is accounted for by a single nondimensional parameter: the ratio of coupling strengths; and (b) the period profile along the AP axis is conserved across species. Thus the model is consistent with the idea that, although the genes involved in pattern propagation in the PSM vary, there is a conserved patterning mechanism across species.

Key words: somitogenesis, clock and wavefront model, Burger's equation,

Accepted manuscript

1. Introduction

Somitogenesis is the highly robust process by which the vertebrate trunk is divided into a series of segments called somites (Gilbert, 1997). Somite formation, which occurs rhythmically from the pre-somitic mesoderm (PSM) in a strict anterior-posterior (AP) sequence, is coincident with PSM growth (Gomez and Pourquié, 2009). As the process of somitogenesis evolves in time, mesenchymal cells in the posterior PSM differentiate into epithelial cells in a strict spatio-temporal manner (Dequéant and Pourquié, 2008). Hence, a posteriorly moving wave of

*murrayp@maths.ox.ac.uk

ACCEPTED MANUSCRIPT

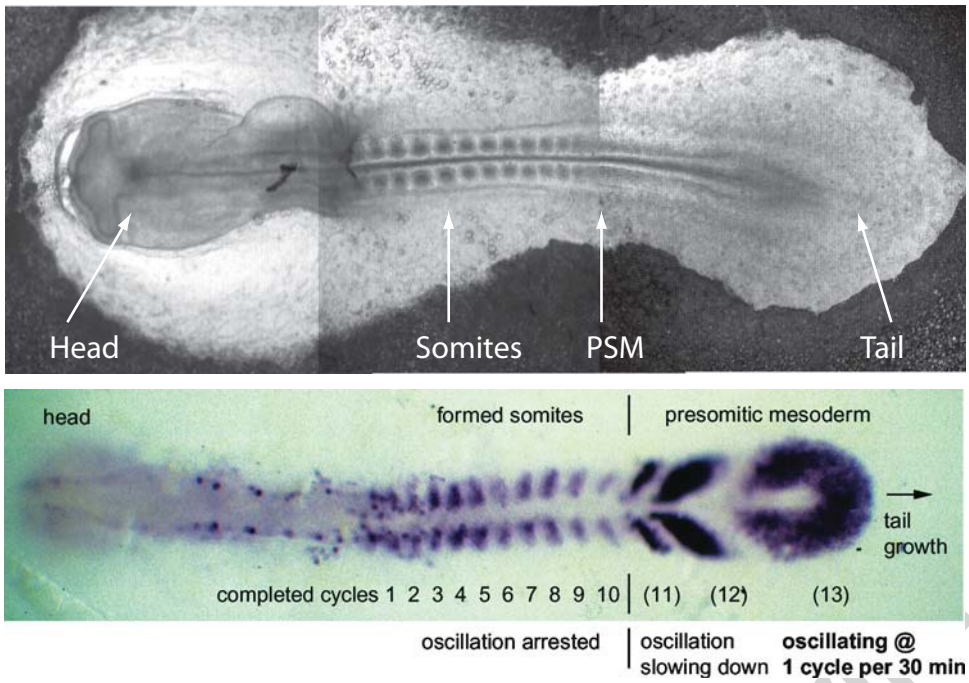

Figure 1: Top: Sequential somite formation in the chick PSM. Image supplied by kind permission of Paul Kulesa, Stowers Institute for Medical Research. Bottom: Patterns of gene expression in the zebrafish PSM illustrated via *in situ* hybridisation (Giudicelli et al., 2007) (permission pending).

differentiation is observed (see Figure 1). One of the key challenges in somitogenesis research is to understand the mechanisms governing the spatio-temporal propagation of this wave of differentiation.

Each cell in the PSM has a segmentation clock whose oscillation frequency is dependent on its relative position along the AP axis (Dequéant et al., 2006). Oscillations in the posterior PSM occur at an approximately constant rate corresponding to the frequency at which somites form (Schröter et al., 2008) but, as the wave of differentiation moves along the PSM, the oscillation frequency of a given cell decreases; somite formation occurs at the spatial position where the oscillations cease. When oscillating components of the somitogenesis clock are examined using techniques such as *in situ* hybridisation (see Figure 1), stripes of gene expression, arising as a result of the variable oscillation frequency along the AP axis, are observed moving anteriorly (Giudicelli et al., 2007). The number of stripes varies between species (Gomez et al., 2008).

Numerous genes and proteins that oscillate at the rate at which somitogenesis occurs have been identified across a number of species. In zebrafish, all known oscillating molecules are downstream regulators of the Notch-Delta signalling pathway (Dequéant and Pourquié, 2008) and it is thought that delayed negative feedback (*i.e.* a given protein inhibits the expression of its corresponding gene with a delay resulting from transcription and translation) plays a fundamental role in regulating the somitogenesis clock (*e.g.* Monk, 2003; Lewis, 2003; Giudicelli et al., 2007). One role of Notch-Delta signalling is to synchronise neighbouring molecular clocks (Horikawa et al., 2006). However, perturbations in the Notch-Delta signalling pathway also influence somite length and oscillation period (Herrgen et al., 2010).

Molecular gradients that travel along the AP axis have been hypothesised to be manifestations of the wavefront of differentiation (Dubrulle et al., 2001). In zebrafish, Fgf mRNA is

ACCEPTED MANUSCRIPT

produced only in the posterior PSM. As these molecules have relatively short protein half-lives, gradients are therefore established along the AP axis that are fixed with respect to the regressing tail of the embryo. However, a causal relationship between the observed travelling gradients and regulation of the cellular oscillations has yet to be established. Detailed quantitative measurements of somitogenesis at the cellular scale and above have recently been undertaken. Giudicelli et al. (2007) have measured the distance between the anteriorly moving stripes of gene expression in zebrafish, Gomez et al. (2008) have made similar measurements in snake, as well as measuring the length of the PSM as somitogenesis progresses; Schröter et al. (2008) have quantified the variation in somite length and oscillator period as somitogenesis proceeds: the former is temperature compensated while the latter decreases with temperature. Herrgen et al. (2010) and Schröter and Oates (2010) have measured relative variation in somite length and oscillator period in somitogenesis mutants. These relatively recent data provide a means of quantitatively testing mathematical models of somitogenesis, of which there is a relatively long history.

Cooke and Zeeman (1976) proposed a 'clock and wavefront' model in which cellular clocks and a moving gradient determined 'when' and 'where' somites form, respectively. The discovery of the molecular components of the somitogenesis clock and moving molecular gradients added significant experimental backing to this model. Baker and co-workers (2008) considered partial differential equation (PDE) models which phenomenologically incorporated both the travelling wavefront and cellular oscillations. These models were derived at the cell population scale and aimed to relate a coarse-grained description of cell-cell communication mechanisms to the formation of pattern. In recent years, given the discovery of molecular clocks and gradients, mathematical models of somitogenesis have focused on capturing the underpinning molecular mechanisms. For example, Lewis and coworkers (Lewis, 2003; Giudicelli et al., 2007) have developed and parameterised models of the molecular clock in zebrafish. These models were applied in a multicellular context by Horikawa et al. (2006), who considered a 1D chain of somitogenesis oscillators coupled together via Notch-Delta signalling. By treating oscillator phase as the dependent variable, Morelli et al. (2009) and Herrgen et al. (2010) have developed a model of intermediary scale between the phenomenological models considered by Cooke and Zeeman (1976) and Baker and co-workers (2008), and the molecular model considered by Horikawa et al. (2006).

A common feature of models attempting to capture the patterning of stripes and somite formation along the AP axis is that a travelling wavefront of differentiation is assumed to exist *a priori* (Tiedemann et al., 2007; Giudicelli et al., 2007; Baker et al., 2008; Morelli et al., 2009; Herrgen et al., 2010). The characteristics of the wavefront, such as the wave speed and profile, are therefore inputs which are crucial to the properties of the emergent patterning behaviour of the respective models. While this modelling assumption is validated, to a certain extent, by observations of travelling molecular gradients of morphogens, such as Fgf and Wnt (Dubrulle et al., 2001), there is not yet definitive evidence that demonstrates a causal relationship between the propagation of the wavefronts and the slowing of cellular oscillations.

1.1. Outline

In this paper we consider a continuum model of a population of somitogenesis oscillators. We focus solely on building a model which accounts for the evolution of a prepattern that determines the positions at which somites form. Our model demonstrates that oscillator coupling is sufficient to establish the emergent patterns observed in somitogenesis. Moreover, a travel-

Accepted manuscript

ACCEPTED MANUSCRIPT

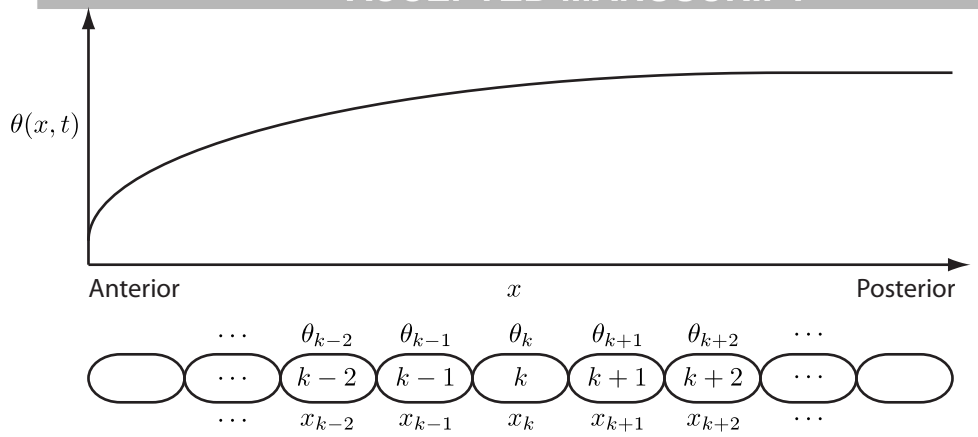

Figure 2: A schematic illustration of the phase profile of a one-dimensional chain of oscillators. Each cell has a spatial coordinate, x_k, and a time-dependent phase, θ_k, that is a readout of the underlying somitogenesis clock. Equation (1) describes how a continuum description of the phase, $\theta(x,t)$, evolves in time as a result of molecular oscillations and oscillator coupling.

ling wave that slows cellular oscillations is an emergent property of the model. As the model is mathematically tractable, we derive expressions for the velocity of the travelling wavefront and its profile. We parameterise the model using experimentally known quantities and subsequently make a number of predictions that are in agreement with available experimental data. The layout of the paper is as follows: in Section 2 we develop, analyse and parameterise the model; in Section 3 we consider numerical solutions of the model and demonstrate an excellent fit with experimental data; in Section 4 we consider experimentally motivated perturbations to the model; in Section 5, using snake as a model organism, we demonstrate how our model can be fitted to *in situ* stripe expression data and, subsequently, parameterise the model using snake, chick and mouse data; and, finally, in Section 6 we conclude with a summary of the main results in this paper and a comparison of our model with similar models in the literature.

2. A phase description of a chain of coupled oscillators

This study is based upon the following PDE that describes how oscillator phase, $\theta(x,t)$, varies in space, x, and time, t (see schematic in Figure 2):

$$\frac{\partial\theta}{\partial t} = \omega + A\frac{\partial^2\theta}{\partial x^2} - B\left(\frac{\partial\theta}{\partial x}\right)^2. \tag{1}$$

The parameter ω represents the rate of phase progression in the homogeneous posterior PSM, and the parameters A and B represent the effects of oscillator coupling arising from cell movement and/or Notch-Delta signalling (Jiang et al., 2000; Uriu et al., 2010). The form of equation (1) can, in principle, be derived explicitly from molecular models of coupled oscillators (Kuramoto, 1981). As we wish to examine the propagation of spatial pattern without explicitly considering embryo growth or pattern initiation, we define the spatial domain $x \in [-\infty, \infty]$ with $x \to -\infty$ and $x \to \infty$ corresponding to the anterior and posterior ends of the embryo, respectively.

Accepted manuscript

ACCEPTED MANUSCRIPT

2.1. A discrete model of coupled oscillators

In order to demonstrate how a chain of discrete oscillators can give rise to the phase equation (1), we consider a chain of phase coupled oscillators (e.g. Murray, 1989) with the dynamics of the j^{th} oscillator given by

$$\dot{\theta}_j = \sum_i \Big[A\sin(\theta_i - \theta_j) + B(\cos(\theta_i - \theta_j) - 1) \Big] + \omega; \qquad j = 1, ..., N, \tag{2}$$

where the sum is taken over nearest neighbours and N is the number of oscillators in the system. The sinusoidal coupling is attractive and synchronising and thus represents Notch-Delta mediated synchronisation (Riedel-Kruse et al., 2007; Özbudak, E. M. and Lewis, J., 2008) while the cosine coupling is repulsive and desynchronising (i.e. it forces neighbouring oscillators out-of-phase with one another). It is worth noting that when $B = 0$ the model is similar to that proposed by Kuramoto (1981) and oscillators synchronise with their nearest neighbours. In contrast, if $A = 0$ the cosine terms force neighbouring oscillators to be completely out-of-phase. Thus the cosine term could originate from a type of coupling similar to that which governs the process of lateral inhibition. When both A and B are non-zero the steady-state phase difference between a pair of neighbouring oscillators is the result of a balance between attractive and repulsive coupling. We note that the model can be written in Kuramoto form be defining

$$\Gamma(\theta) = A\sin\theta + B(\cos\theta - 1), \tag{3}$$

in which case

$$\dot{\theta}_j = \sum_i \Gamma(\theta_i - \theta_j) + \omega; \qquad j = 1, ..., N, \tag{4}$$

and leave it as an open question to determine the molecular models that yield an appropriate $\Gamma(\theta)$ (we refer the reader to A for a demonstration of how a molecular model could yield equation (1)). The equivalence of equations (1) and (2) can be demonstrated by assuming that neighbouring oscillators are close together in phase, *i.e.* $|\theta_i - \theta_{i-1}| \ll 2\pi$, expanding the sine and cosine terms and taking the continuum limit (see B).

2.2. Boundary conditions and model analysis

In the posterior PSM oscillations are synchronous (*i.e.* the phase of neighbouring oscillators is spatially homogeneous, see Figure 1), hence we impose the boundary condition

$$\left.\frac{\partial\theta}{\partial x}\right|_{x\to\infty} = 0. \tag{5}$$

As the oscillation rate tends to zero in the anterior PSM, we impose the boundary condition

$$\left.\frac{\partial\theta}{\partial x}\right|_{x\to-\infty} = \sqrt{\frac{\omega}{B}}, \tag{6}$$

which is the stable steady-state of equation (1). We define the initial condition:

$$\theta(x, 0) = \theta_0(x). \tag{7}$$

Accepted manuscript

ACCEPTED MANUSCRIPT

Upon differentiation of equation (1) with respect to the variable x, and defining

$$\Psi(x,t) = \frac{\partial \theta}{\partial x}, \tag{8}$$

we obtain Burger's equation for Ψ, *i.e.* the nonlinear advection-diffusion equation:

$$\frac{\partial \Psi}{\partial t} + 2B\Psi\frac{\partial \Psi}{\partial x} = A\frac{\partial^2 \Psi}{\partial x^2}, \tag{9}$$

which has applications in a range of fields such as traffic flow modelling (*e.g.* Whitham, 1974; Kuramoto, 1981; Ockendon et al., 2003). This model has a travelling wave solution, and, defining the travelling wave coordinate $y = x - Ut$, together with the boundary conditions (5) and (6), the wave velocity is

$$U = \sqrt{\omega B}. \tag{10}$$

Ahead of the wave (*i.e.* in the posterior PSM) the solution is

$$\theta(x,t) \sim \omega t, \tag{11}$$

which corresponds to spatially homogeneous temporal oscillations (the solution has no dependence on x), while behind the wave

$$\theta(x,t) \sim \sqrt{\frac{\omega}{B}}x, \tag{12}$$

hence the solution is independent of t. Assuming that phase is determined modulo 2π, a spatial pattern with wavelength

$$S_{exp} = 2\pi\sqrt{\frac{B}{\omega}}, \tag{13}$$

corresponding to somite length, is obtained.

Assuming dynamic equilibrium in a reference frame moving with velocity U relative to the laboratory frame, our model has one independent variable, y, which is the distance between a given point and the midpoint of the phase gradient. We obtain the following results (depicted in Figure 3): the phase gradient is

$$\Psi(y) = \frac{\sqrt{\frac{\omega}{B}}}{1 + e^{\frac{\sqrt{\omega B}y}{A}}}; \tag{14}$$

the angular frequency is

$$\Omega(y) = \omega\left(1 - \frac{1}{1 + e^{\frac{\sqrt{\omega B}y}{A}}}\right); \tag{15}$$

the oscillation period is

$$T(y) = \frac{2\pi}{\omega}\left(1 + e^{-\frac{\sqrt{\omega B}y}{A}}\right); \tag{16}$$

Accepted manuscript

ACCEPTED MANUSCRIPT

and the wavelength of the pattern, defined such that $\theta(y+S/2)-\theta(y-S/2)=2\pi$, is

$$S(y)=2\pi\sqrt{\frac{B}{\omega}}\left(1+\frac{A}{\pi B}\sinh^{-1}\left(\sinh\frac{\pi B}{A}e^{\frac{\sqrt{\omega B}y}{A}}\right)\right). \tag{17}$$

Equations (10)-(17) describe quantities that are experimentally measurable. Moreover, consider a solution to equation (9) that is in dynamic equilibrium (*i.e.* the wave moves with constant wave speed $U=\sqrt{\omega B}$ with oscillation frequency profile given by equation (15)): the time taken for the wave to travel a distance X is $X/\sqrt{\omega B}$. Letting $y=X/2-\sqrt{\omega B}t$ in equation (15) and integrating over t for a time $X/\sqrt{\omega B}$, we obtain that the change in phase for a stationary cell as the wavefront passes over it (assuming the centre of the wavefront is initially at $x=0$) is

$$\Delta\theta=\frac{X}{2}\sqrt{\frac{\omega}{B}}. \tag{18}$$

In order to determine the phase lag induced by the travelling wavefront, we subtract equation (18) from the phase change undergone by a freely oscillating cell (*i.e.* $X\sqrt{\omega/B}$) and divide by 2π to obtain that the number of moving stripes observable in a region of width X centred at the midpoint of the phase gradient is given by

$$N_s=\frac{X}{4\pi}\sqrt{\frac{\omega}{B}}=\frac{X}{2S_{exp}}. \tag{19}$$

2.3. Parameter estimation

We use data from zebrafish (Giudicelli et al., 2007) in order to initially parameterise the model. At $T=30$ ℃ the oscillation period in the posterior PSM, T_{exp}, is 30 minutes. Therefore, using equation (11) we obtain

$$\omega=\frac{2\pi}{T_{exp}}. \tag{20}$$

We approximate that the somite length, S_{exp}, is approximately six cell diameters (c.d.) at the seven somite stage ((Schröter et al., 2008) measure $53\mu m$ while Gomez et al. (2008) measured $75\mu m$). As one somite forms for every clock cycle in the PSM we assume that the wave speed is given by S_{exp}/T_{exp}. Hence substitution into equation (10) leads to

$$B=\frac{S_{exp}^2}{2\pi T_{exp}}. \tag{21}$$

In order to determine the parameter A we use equation (14) to determine the length scale over which the wavefront varies. Making a linear approximation to the gradient at $y=0$, where $d\Psi/dy$ takes its maximal value of $\omega/4A$ (see schematic in Figure 4), we find that the length scale, L_{exp}, over which the phase gradient varies is given by

$$L_{exp}=\frac{4A}{\sqrt{\omega B}}. \tag{22}$$

Accepted manuscript

ACCEPTED MANUSCRIPT

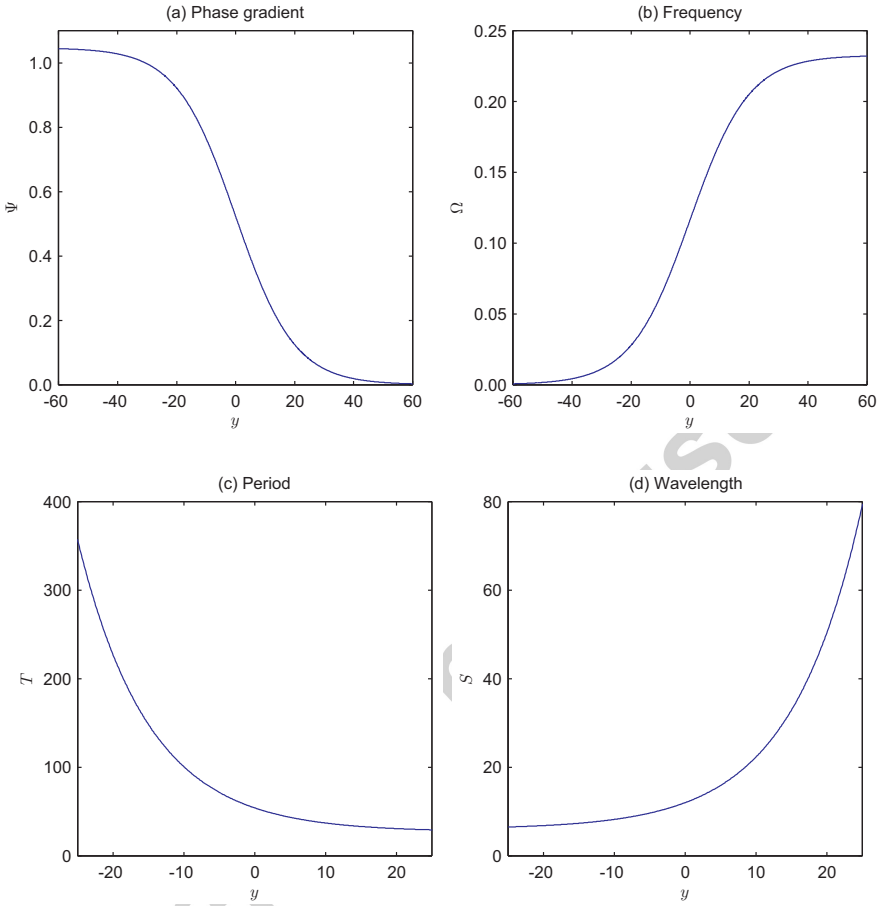

Figure 3: Model variables (equations (14) - (17)) plotted in the travelling wave reference frame. $y = 0$ corresponds to the centre of the phase gradient and y increases posteriorly. (a) The phase gradient, $\Psi(y)$, (b) the oscillation frequency, $\Omega(y)$, (c) the oscillation period, $T(y)$, and (d) the pattern wavelength, $S(y)$, plotted against y. $(\omega, A, B) = (0.23, 2.22, 0.21)$.

ACCEPTED MANUSCRIPT

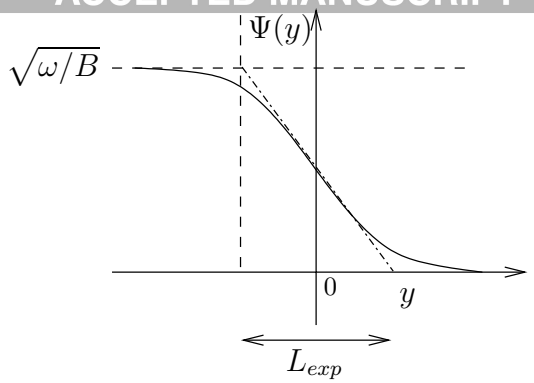

Figure 4: A schematic illustration of how the length scale of the phase gradient is defined. The phase gradient attains its maximum of $\Psi = \sqrt{\omega/B}$ anteriorly and its minimum $\Psi = 0$ posteriorly. The straight dot-dashed line represents a linear approximation to the phase gradient at the origin, from which the length scale is determined.

Given an experimental measurement of the length scale of the phase gradient, equation (22) can be rearranged to yield

$$A = \frac{L_{exp} S_{exp}}{4 T_{exp}}. \tag{23}$$

In the Giudicelli et al. (2007) study, the PSM length, L_{PSM}, is defined to be the distance from the tail end of the notochord to the anterior end of the PSM and is measured to be eight times the somite length, *i.e.* $L_{PSM} = 8 S_{exp}$. Using L_{PSM} as an approximation to the length scale of the phase gradient and defining unit length to be one cell diameter, we approximate that $(T_{exp}, S_{exp}, L_{exp}) = (30\text{mins}, 6 \text{ c.d.}, 48 \text{ c.d.})$ for zebrafish somitogenesis at the 7-15 somite stage at $T = 30$ ℃ (Giudicelli et al., 2007), in which case our model parameters take the values $(\omega, A, B) = (0.21, 2.40, 0.19)$.

We note that in the classic interpretation of Cooke and Zeeman's clock and wavefront model the somite length is related to the clock period by

$$S_{exp} = v T_{exp}, \tag{24}$$

where v is the constant wavespeed of the travelling wavefront. In our model the wavespeed is a function of the oscillation frequency, ω, and the coupling parameter B. After substitution using equation (10) we find that

$$S_{exp} = \sqrt{2\pi B}\sqrt{T_{exp}}. \tag{25}$$

This result has important biological implications: (a) the somite length scales with the square root of the clock period; and (b) knowledge of how a perturbation alters oscillator period is insufficient to describe the effect on somite length (*e.g.* if an experimental perturbation increases the oscillation frequency by a certain factor but also increases the coupling parameter B by the same factor then somite length remains constant).

3. Model validation and predictions

In this section we examine numerical solutions of equation (1) together with boundary conditions (5) and (6) and compare them with experimental data (where available). In Figures

Accepted manuscript

ACCEPTED MANUSCRIPT

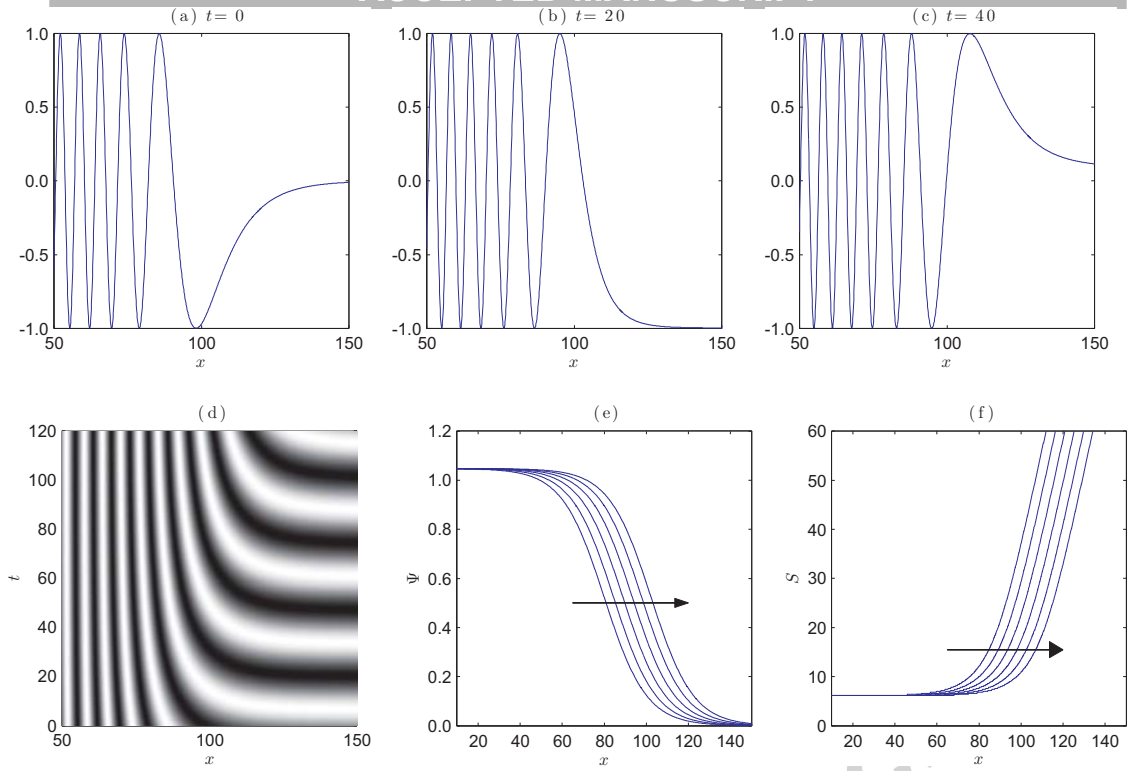

Figure 5: Plots of the numerical solution of equations (1)-(6). (a)-(c) $\sin(\theta)$ plotted against x at $t = \{0, 20, 40\}$ minutes. (d) $\sin(\theta)$ plotted against x and t. (e) The phase gradient, $\Psi(x,t)$, plotted against x at $t = \{0, 20, 40, 60, 80, 100\}$ minutes. The arrow indicates the direction of travel of the wavefront. (f) The pattern wavelength, $S(x,t)$, plotted against x at $t = \{0, 20, 40, 60, 80, 100\}$ minutes. Ahead of the wave (large x, small t) the phase increases at rate ω but is spatially constant. Behind the wave (large t, small x) the pattern oscillates in space with wavelength S_{exp} but is constant in time. x, the spatial coordinate in the laboratory frame, increases posteriorly. Parameter values: $(\omega, A, B) = (0.21, 2.40, 0.19)$.

5 (a)-(c) $\sin(\theta)$ is plotted against x at a series of times[1]. The initial conditions are taken to be the steady-state phase gradient given by equation (14). For large x the solution oscillates in time, $\theta = \omega t$, while for small x the solution is time independent but takes the form $\theta = \sqrt{\omega/B}x$ (see Figure 5(d)). The nature of the travelling wave can be clearly seen in Figures 5(e)-5(f), where the phase gradient and pattern wavelength are plotted against x at increasing times. As expected, the travelling wave moves with velocity $U = \sqrt{\omega B}$ and the wavelength of the pattern, corresponding to somite length, is six cell diameters.

Giudicelli et al. (2007) have measured the distance between the anteriorly-moving stripes of gene expression (*e.g.* see Figure 1) and in Figure 6(a) we demonstrate good agreement between their data and the expression of wavelength defined in equation (17) with the parameters as chosen in Section 2.3. Whilst this satisfactory fit suggests that L_{PSM} is a good approximation to the length scale of the phase gradient, we can formalise this argument by performing a least squares fit of equation (17) to the stripe expression data. In order to do this we must rescale our model such that L_{PSM} is unit length, in which case the expression for the stripe wavelength

[1] $\sin\theta(x)$ rather than $\theta(x)$ is plotted, as the range of the former function is defined on the domain $[-1, 1]$ which can be qualitatively compared with concentration profiles from *in situ* staining experiments (Morelli et al., 2009).

ACCEPTED MANUSCRIPT

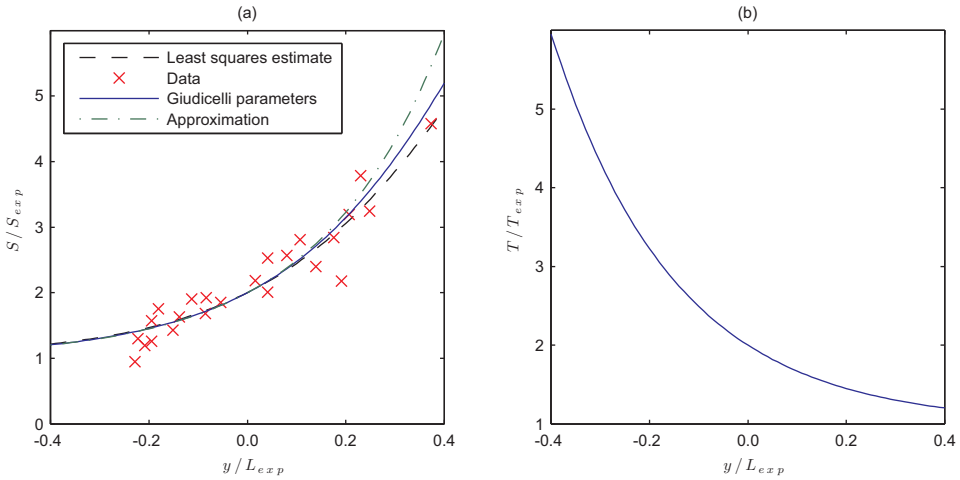

Figure 6: Comparison of model predictions (lines) with experimental data (markers). y, the spatial coordinate in the travelling reference frame, increases posteriorly. (a) Rescaled wavelength, $S(y)/S_{exp}$ plotted against rescaled spatial coordinate, y/L_{exp}. Solid line: equation (17) with parameters estimated using zebrafish data (Giudicelli et al., 2007); dashed line: least squares fit using equation (26); dot-dashed line: least squares estimate using equation (27). (b) Prediction of rescaled oscillation period, $T(y)/T_{exp}$, (see equation (16)) plotted against rescaled spatial coordinate, y/L_{exp}.

is given by

$$\frac{S(y)}{S_{exp}} = 1 + \frac{c_1 L_{PSM}}{2S_{exp}} \sinh^{-1}\left(\sinh\frac{2S_{exp}}{c_1 L_{PSM}} e^{\frac{4(y-c_2)}{c_1}}\right), \tag{26}$$

where $c_1 = L_{exp}/L_{PSM}$ and $c_2 = y_0/L_{PSM}$. For the Giudicelli et al. (2007) zebrafish data we obtain that $\{c_1, c_2\}=\{1.08, -0.2\}$, *i.e.* L_{exp} is approximately 10% greater than the measurement L_{PSM} used in the Giudicelli et al. (2007) study and the centre of the phase gradient lies approximately one somite length anterior to the centre point of their reference frame. We note that the quality of the fit could be improved via inclusion of more data points anterior to the origin in the Giudicelli et al. (2007) coordinate system (see the posterior bias of the data points relative to the centre of the phase gradient).

A calculation of the number of stripes of gene expression in the range $[-L_{exp}/2, L_{exp}/2]$ using equation (19) predicts that $N_s = 4$. In other words, the phase of a cell at position $-L_{exp}/2$ relative to the centre of the travelling wave lags the oscillations in the posterior PSM by approximately four cycles owing to the decreased frequency rate induced by the posteriorly moving wavefront.

In order to derive a simple relationship between the stripe expression and period profiles, we use the approximation $\sinh(x) = \sinh^{-1}(x) = x$, which is reasonable for $|x| < 1$, in equation (17) and obtain that

$$S(y) = 2\pi\sqrt{\frac{B}{\omega}}\left(1 + e^{\frac{\sqrt{\omega B}y}{A}}\right). \tag{27}$$

This is valid so long as $\pi B/A < 1$ and $y < A/\sqrt{\omega B}\ln(1/\sinh(\pi B/A)) = 16.5$. As $\pi B/A = 0.24$ the first approximation holds as result of the greater strength of attractive coupling, while the second approximation holds only in the anterior 3/4 of the posterior PSM.

ACCEPTED MANUSCRIPT

Combining equations (16) and (27) we deduce that the oscillation period is related to the stripe wavelength data (Figure 1) via the relationship

$$\frac{T(y)}{T_{exp}} = e^{\frac{-4y}{L_{exp}}} \frac{S(y)}{S_{exp}}. \tag{28}$$

This expression can be compared with the expression

$$\frac{T(y)}{T_{exp}} = \frac{1}{1 + \left(\frac{y}{L_{exp}} - \frac{1}{2}\right) \frac{S(y)}{S_{exp}}}, \tag{29}$$

derived by Giudicelli et al. (2007), which has been used to infer temporal information regarding the clock from the spatial stripe pattern. We note that both expressions predict that the clock period varies inversely with the stripe wavelength, *i.e.* in the spatially homogeneous posterior PSM oscillation periods are minimised, while in the spatially patterned anterior PSM the oscillation periods become large. A key difference between the models is that equation (29) predicts that the clock period tends to infinity at $y = -L_{exp}/2$ while equation (28) predicts an exponential increase in clock period.

4. Experimental perturbations

We now test our model against a series of experiments in which oscillator coupling, somite size and the rate at which somitogenesis proceeds are perturbed.

4.1. Transplant of 'out of phase' cells

In order to demonstrate the synchronous effects of coupling between oscillators in the PSM, Horikawa et al. (2006), using zebrafish as a model organism, isolated a group of cells from a wild-type donor embryo and transplanted them into the posterior PSM of a host embryo. Within three oscillation cycles the explanted cells, which were originally out of phase with the host cells, had completely synchronised with those in the host PSM.

In order to investigate this phenomenon, we compare two numerical solutions of our model which had different initial conditions: the first solution has initial conditions that are in dynamic equilibrium (phase gradient given by equation (14)), while the second solution is a perturbation of the first: a small patch of cells are initially out-of-phase with the bulk posterior PSM. The numerical results in Figure 7(b), in which the difference between perturbed and unperturbed solutions is plotted against x and t, are in qualitative agreement with the experimental findings of Horikawa et al. (2006): the introduced cells resynchronise with the posterior PSM with no effect on somite length (see Figure 7(a)).

4.2. Transplant of cells overexpressing Delta ligands

Horikawa et al. (2006) performed a further set of experiments in which a small number of cells that had been treated with Her morpholinos were transplanted into one side of a host PSM. As Her negatively regulates Delta transcription, Horikawa et al. (2006) argue that these cells should express high levels of Delta ligands and therefore transplantation into a host embryo should result in modified oscillations in the host cells. They found that somites which formed adjacent to the transplanted cells were smaller than those in the control experiment. Moreover, all somites that formed posterior to the transplanted cells were shifted anteriorly relative to the

Accepted manuscript

ACCEPTED MANUSCRIPT

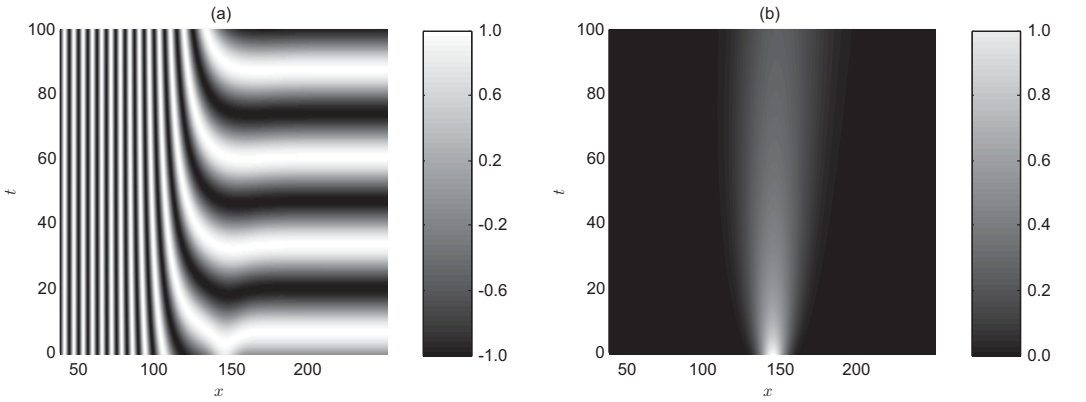

Figure 7: Dissipation of a phase perturbation introduced at $(x, t) = (145, 0)$. (a) The perturbed solution plotted against x and t. (b) The perturbation plotted against x and t.

control side of the embryo. From these experimental results Horikawa et al. (2006) concluded that Notch-Delta signalling influences somite length and spatial position.

As it is not clear from the experimental study which of the parameters A, B or ω are modified by the overexpression of Notch ligands, here we suppose that the perturbation decreases the parameter ratio B/ω in the region $x \in [126, 136]$ (see Figure 8). Accordingly, at $x \sim 130$ we observe a local decrease in pattern wavelength (corresponding to somite length). Moreover, in the region posterior to the varying parameter (where the parameter ratio B/ω takes the wild type value), the pattern wavelength increases and subsequent somite length returns to normal. However, as observed experimentally, the somite pattern is shifted anteriorly along the AP axis (see Figure 8(b)). We note that the effect of perturbing the parameter A on the phase gradient is transient and therefore not observable given the experimental protocol, hence we have not considered whether or not it is modified in the Horikawa et al. (2006) explant experiment.

In our model framework a spatially localised increase in the parameter ratio B/ω, corresponding to downregulation of Notch ligand expression on the cell surface, will result in the formation of larger somites and a corresponding phase lag in the perturbed side of the embryo (see numerical simulation in Figure 9). We note that Herrgen et al. (2010) have recently shown that mutants for Delta ligands and Notch receptors have increased somite lengths and oscillator periods, which is consistent with the idea that activation of the Notch pathway decreases the parameter ω.

4.3. Temperature compensation

Schröter et al. (2008) have demonstrated that the rate at which somitogenesis proceeds increases with temperature while somite length is temperature independent. In order for these observations to be consistent with Cooke and Zeeman's 'clock and wavefront' model, the velocity of the travelling wavefront must be temperature dependent.

In our model framework, temperature compensation of somite length arises naturally upon the assumption that each of the parameters ω, A and B scale similarly with temperature, T, such that

$$\omega = \omega_0 h(T^\lambda), \qquad A = A_0 h(T^\lambda), \qquad B = B_0 h(T^\lambda), \tag{30}$$

Accepted manuscript

ACCEPTED MANUSCRIPT

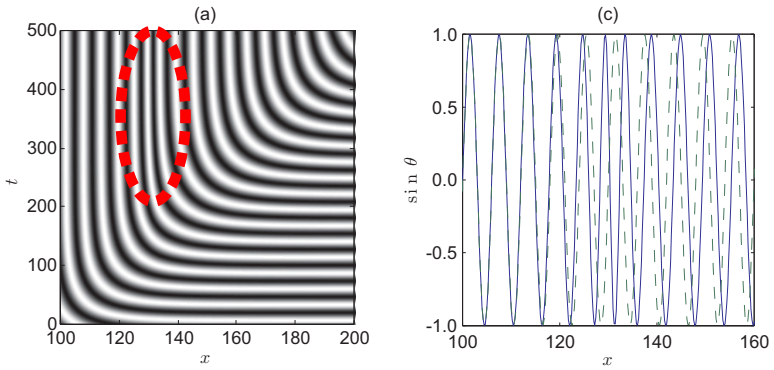

Figure 8: Simulation of Notch-ligand expressing cell implant experiment. In the range $x \in [126, 136]$ the parameter ratio B/ω is decreased by a factor of ten. (a) $\sin\theta$ plotted against x and t. At $x \sim 130$ the pattern wavelength is locally decreased corresponding to the formation of smaller somites. (b) $\sin\theta$ plotted against x at $t = 900$: dashed line (unperturbed solution), solid line (perturbed solution).

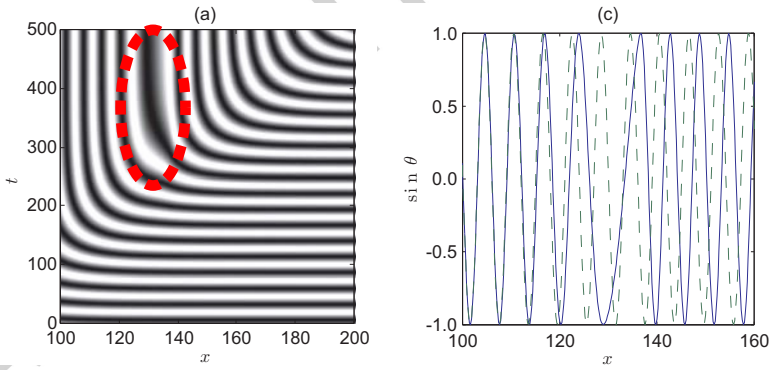

Figure 9: In the range $x \in [126, 136]$ the parameter ratio B/ω is increased by a factor of ten to simulate the introduction of cells with reduced Notch ligand cell surface expression. (a) $\sin\theta$ plotted against x and t. At $x \sim 130$ the pattern wavelength is locally increased corresponding to the formation of a larger somite. (c) $\sin\theta$ plotted against x at $t = 900$: dashed line (unperturbed solution), solid line (perturbed solution).

ACCEPTED MANUSCRIPT

Figure 10: A schematic diagram comparing different measurements of length scales in the PSM. Top: in snake, Gomez et al. (2008) use the anterior boundary of the Mesogenin1/Mesp0 expression domain (hatched) to define the determination wavefront and the distance from the last formed somite to the posterior tip, L_{PSM}, of the embryo to define the length scale of the PSM. In zebrafish, Giudicelli et al. (2007) use the distance from the last formed somite to the tail end of the notochord, L^*_{PSM}, to define the length scale of the PSM. Bottom: stripe expression data together with equation (26) can be used to determine the length scale of the phase gradient, L_{exp}, and its centre point, y_c.

where h is some scaling function and λ a scaling parameter. Substituting the scaling relationships in equations (30) into equation (10), we find that the wave speed

$$U = \sqrt{\omega B} \propto \sqrt{h(T^\lambda)^2} \propto h(T^\lambda), \tag{31}$$

scales proportionally with $h(T^\lambda)$. However, recalling from equation (13), behind the wavefront somite length is given by

$$S_0 = 2\pi\sqrt{\frac{B}{\omega}}, \tag{32}$$

which is independent of T. As the clock oscillation rate scales approximately linearly with temperature (Schröter et al., 2008), we assume that the parameters A and B have a similar scaling. Hence, as the environmental temperature increases, individual somitogenesis clocks oscillate at a faster rate but the wave speed also increases such that somite length remains fixed. A similar argument applied to equation (19) suggests that the number of moving stripes observed along the AP axis should also be temperature independent.

5. Applying the model to other species

We now describe how our model can be: (a) used to unambiguously define a travelling reference frame in the PSM; (b) fitted to data from other species; and (c) used to explain variation in stripe expression profiles across different species.

5.1. Parameter fitting to in situ stripe expression data

There is disparity in the literature as to how the length of the posterior PSM is defined across species (see schematic diagram in Figure 10). Anteriorly, the position of the last formed somite has been used to define the origin of a moving coordinate system (Gomez et al., 2008), while, posteriorly, the posterior tip of the PSM (Gomez et al., 2008) or the position of the notochord (Giudicelli et al., 2007) have been used to define unit length. Using *in situ* stripe expression

Accepted manuscript

ACCEPTED MANUSCRIPT

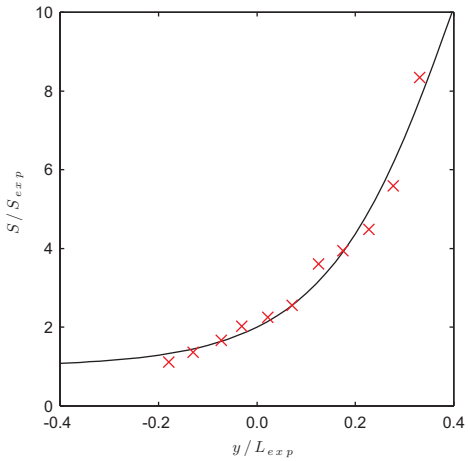

Figure 11: The distance between stripes of Lunatic Fringe expression plotted along the AP axis (markers). Data taken from snake Gomez et al. (2008). Fitting equation (26) (solid line) we find that $L_{exp} = 0.64$, $y_c = -0.23$.

	snake	mouse	chick	zebrafish	unit
S_{exp}	4.8	11.5	15.0	7.5	c.d.
T_{exp}	100	120	90	30	min
L_{PSM}	99.4	63.9	78.9	68.0	c.d.
$L_{exp}{}^*$	70.2	45.1	55.7	48.0	c.d.
ω	0.06	0.05	0.07	0.21	min^{-1}
A	0.83	1.08	2.31	2.99	$\text{c.d.}^2\ \text{min}^{-1}$
B	0.03	0.17	0.40	0.30	$\text{c.d.}^2\ \text{min}^{-1}$
$\gamma = \pi B/8A$	0.02	0.06	0.07	0.04	Nondim
N_s	7.3	2.0	1.9	3.2	Nondim

Table 1: Data taken from Gomez et al. (2008). * In the absence of experimental measurement of L_{exp} we have assumed that the scaling relationship between L_{PSM} and L_{exp} is the same in chick and mouse as it is in zebrafish.

data our model can unambiguously solve this problem. Consider the data presented in Figure 11. Using a least squares fitting algorithm we fit equation (26) to the stripe expression data and obtain estimates for the somite length, the centre of the phase gradient, y_c, and the length scale of the phase gradient. For example, using the snake data from Gomez et al. (2008) we obtain that $L_{exp} = 0.64 L_{PSM}$ with $y_c = -0.23 L_{PSM}$, where L_{PSM} is unit length in the experiment, *i.e.* the length scale of the phase gradient is approximately two thirds the length of the PSM while the centre of the phase gradient is $0.23 L_{PSM}$ anterior to the centre of the coordinate system used in the experiment. Again we note the posterior bias of the data points relative to the centre of the phase gradient. Applying such a measurement technique to stripe expression data as somitogenesis proceeds would allow quantification of how L_{exp} varies throughout somitogenesis.

5.2. Comparing species

In Table 1 we present measurements of L_{exp}, T_{exp} and S_{exp} taken from zebrafish, corn snake, chick and mouse (Gomez et al., 2008) and the corresponding values of the model parameters A, B and ω. Our model suggests that the variation in PSM patterns found across different species

Accepted manuscript

ACCEPTED MANUSCRIPT

is due to different ratios of the coupling parameters A and B. For example, the strength of repulsive coupling in snake is relatively much less than in zebrafish, thus in snake we expect to observe a longer PSM and smaller somites. This argument becomes clearer upon non-dimensionalising the model as follows:

$$\hat{x} = \frac{x}{L_{exp}}, \qquad \hat{t} = \frac{t}{T_{exp}}. \tag{33}$$

With these substitutions, equation (1) takes the form

$$\frac{\partial \theta}{\partial \hat{t}} = \gamma \frac{\partial^2 \theta}{\partial \hat{x}^2} - 16\gamma^2 \left(\frac{\partial \theta}{\partial \hat{x}}\right)^2 + 1, \tag{34}$$

where the nondimensional parameter $\gamma = S_{exp}/4L_{exp} = \pi B/8A$, *i.e.* the ratio of the somite length to the length scale of the phase gradient. With this rescaling the clock period and PSM length are normalised across species and variation in patterning across species arises through variation in the parameter γ. Thus in snake the wave moves relatively slower than in zebrafish (wavespeed $= 4\gamma$) yielding smaller somites.

With the given dimensional scalings, the period of oscillation along the moving wavefront (derived in dimensional units in equation (16)) is given in nondimensional form by the expression

$$T(y) = 1 + e^{-4y}. \tag{35}$$

Note that this expression is independent of γ, implying that the non-dimensional period profile remains constant (even as γ varies across species (see Table 1)). The expression in equation (35) has previously been plotted in Figure 6(b) ($T(y)$ is rescaled with T_{exp} and y is rescaled with L_{exp}) but the analysis in this section predicts that data from other species (when nondimensionalised appropriately) should also lie upon the predicted exponential curve.

The number of stripes moving along the posterior PSM, defined in equation (19), can be rewritten as

$$N_s = \frac{1}{8\gamma}. \tag{36}$$

Note that for zebrafish $\gamma = 0.04$, hence we obtain ~ 3 stripes moving along a displacement of 20 cell diameters on either side of the moving wavefront. In Table 1 we present predictions for the number of moving stripes observed in chick, mouse and snake.

6. Discussion

In 1976, Cooke and Zeeman proposed a clock and wavefront theory of somite formation which was remarkably insightful given the available knowledge of the time. In the meantime, the core components of their model, clocks with anteriorly decreasing frequencies and a posteriorly moving travelling wavefront, have been identified experimentally. However, a number of key issues remain unsolved, such as the identification of a core oscillator and of a causal molecular link between the observed molecular gradients and the slowing of clock oscillations.

In this paper we present a clock and wavefront mechanism of patterning for somite formation that is consistent with the Cooke and Zeeman model: a travelling wavefront slows clock

Accepted manuscript

ACCEPTED MANUSCRIPT

oscillations, one somite is formed for each clock cycle and somites have rostro-caudal polarity. However, the clock and wavefront are not separate entities but, rather, the wavefront is a gradient in clock phase.

A key conclusion from our study is that a minimal number of processes, *i.e.* attractive and repulsive oscillator coupling, are sufficient to explain a wide number of experimental observations in the somitogenesis system. We highlight that, while there is experimental evidence for synchronising coupling during somitogenesis, we are speculating as to the presence of the repulsive oscillator coupling. However, we note that one possible source of the repulsive coupling could be related to Notch-mediated lateral inhibition, thus the oscillator coupling in our model could be thought to originate from a combination of the synchronising and lateral-inhibiting components of the Notch-Delta signalling pathway. A further caveat that must be attached to our model is that we have treated the propagation of the phase gradient as being an autonomous process, while, in reality, the axis elongation, molecular gradient and phase gradient velocities must be coupled (*e.g.* it has been observed that perturbations to the Fgf and Wnt gradients can influence clock oscillation patterns (*e.g.* Dubrulle et al., 2001; Gibb et al., 2009)). We expect that coupling between the phase and molecular gradients could be introduced into our model by allowing the parameters A, B and ω to be functions of the molecular gradients but have not addressed this issue in the current study.

From a biological perspective, this study proposes that there need not be an, as yet elusive, molecular connection coupling the observed travelling molecular gradients to the slowing of clock oscillations. Rather, the slowing of oscillations may be a function of nonlinear cell-cell coupling, perhaps mediated via nonlinear interactions in the Notch-Delta signalling network. Moreover, variation in the cell-cell coupling networks (*i.e.* in the relative strengths of linear and nonlinear coupling) can explain the variation in PSM patterns observed in different species. In order to validate this hypothesis, we use the model to make a number of quantitative predictions, namely the pattern wavelength profiles and the number of moving stripes of gene expression along the AP axis, which we have subsequently verified using published experimental data. Furthermore, we predict the form of the oscillation period profile along the AP axis and that both period and stripe wavelength profiles along the AP axis are, given appropriate rescaling, conserved amongst different vertebrate species.

The pattern wavelength profile along the AP axis represents a key prediction of our model (which we have validated using zebrafish *in situ* expression profiles). Moreover, using snake *in situ* expression profiles, we have demonstrated how the model can be fitted in order to unambiguously define a reference frame along the AP axis. As a result of embryo length variability and the dependency of PSM length on somite stage (Gomez et al., 2008; Schröter et al., 2008), published stripe expression data are typically plotted against a rescaled PSM length. We note that our model could be fitted to more fine-grained data (*i.e.* non-rescaled stripe expression data from different somite stages) in order to define the length scale of the phase gradient as somitogenesis proceeds. It would be intriguing to compare such a measurement with the measurements of the PSM length considered by Gomez et al. (2008) and Schröter et al. (2008), in order to investigate how the length scale and location of the phase gradient varies with the changing length scale of the PSM. We also note that while we have assumed an infinitely long, one-dimensional spatial domain in order to derive analytic expressions for quantities such as the stripe expression profile, qualitative and many quantitative features of the model remain unchanged upon the inclusion of more biologically realistic geometries (data not shown). Moreover, the emergent patterns described in this study are unchanged upon replacement of

Accepted manuscript

ACCEPTED MANUSCRIPT

the anterior boundary condition $\partial\theta/\partial y = \sqrt{\omega/B}$ with a Dirichlet condition in which θ assumes a fixed value. This latter boundary condition may be more appealling from a biological perspective as it requires that cells at the anterior boundary do no oscillate, rather than the specification of a spatial gradient.

We have demonstrated that our model is in qualitative agreement with the resynchronisation experiments conducted by Horikawa et al. (2006) but note that a quantitative comparison between our model and data from resynchronisation experiments would allow independent measurement of the coupling parameters A and B, thereby either supporting or refuting our hypothesis that oscillator coupling plays a key role in the propagation of the phase gradient along the AP axis. We have also shown that our model is consistent with the Horikawa et al. (2006) experiment in which locally increased surface expression of Delta ligands modifies both somite size and the position of the wavefront. In a future study we will quantitatively analyse perturbed phenotypes by combining the phase description developed in this paper with a description of cell movement in the PSM.

One of the key predictions of our model is that the velocity of the phase gradient is determined by the expression $v = \sqrt{\omega B}$, hence somite length is proportional to the square root of the clock period. This prediction appears at first sight to be in direct contradiction with recent experiments in the Hes6 mutant (Schröter and Oates, 2010), where the velocity of the wavefront was measured to be the same as in the wild type embryo while the somite length and somitogenesis period both increased by a factor of 1.07, data that are consistent with the classical relationship $S = vT$. How can our model be reconciled with these observations? If we suppose that the Hes6 mutation decreases ω by a factor of 1.07 and increases B by the same factor (*i.e.*, the Hes6 mutation affects oscillator coupling as well as frequency) then our model yields the observed changes in somitogenesis period and somite length. Moreover, the phase-gradient velocity is the same as in the wild-type case. One might then argue that the classical model is favourable as it can explain the data in a simpler manner. However, in a recent study Herrgen et al. (2010) have measured the somite lengths and somitogenesis periods in a range of Notch-Delta mutants. Intriguingly, the wavefront velocity is measured to be unchanged in the mutant embryos while, unlike the Hes6 mutant, the somite lengths and period change by non-constant factors. Hence, the classical interpretation of Cooke and Zeeman's model cannot explain the Notch-Delta mutant observations. This topic will be investigated further in a future publication.

It remains to be discovered how the phase equation (1) can be derived from biologically plausible models of coupled somitogenesis clocks. In general, equation (1) can be derived from systems of molecular oscillators in the limit of weak coupling (Kuramoto, 1981). However, it is not clear *a priori* what types of molecular models can be coarse-grained such that equation (1) can be used to describe patterning in the molecular oscillations. In this study we have considered a toy model of coupled cellular oscillators (a $\lambda - \omega$ system) as the model parameters have clear meaning at the phase description (*e.g.* the parameter P represents strength of attraction to the limit cycle). Our results hint at some properties that more complex oscillators should possess in order that the phase description considered in this paper is a valid description of oscillation patterning: (a) nonlinear cell-cell coupling is required to slow oscillations along the AP axis; and (b) strong limit cycle attraction is required in the uncoupled model such that cell-cell coupling serves to slow the rate of oscillation without the oscillator moving away from the limit cycle.

We note that Morelli et al. (2009) have considered a phase description of PSM oscillators in which coupling is represented by a diffusion term and a travelling wave in oscillation frequency is

Accepted manuscript

ACCEPTED MANUSCRIPT

imposed. Our model can be thought of as an extension of this framework, in that by considering higher order oscillator coupling, the travelling wave oscillator frequency profile becomes an emergent model property.

Finally, we propose that the parameters A and B, which represent the strengths of linear and quadratic coupling, could be independently measured using quantitative analysis of resynchronisation experiments. Independent experimental measurements of these coupling strengths, and their variation across different species, would provide a clear means to validate/refute the mechanism for the clock and wavefront model hypothesised in this study.

Acknowledgements

PJM and REB acknowledge the support of the Engineering and Physical Sciences Research Council through an EPSRC First Grant to REB. PKM was partially supported by a Royal Society-Wolfson Research Merit Award. PJM acknowledges the support of St Hughs College, Oxford.

References

Baker, R. E., Schnell, S., Maini, P. K., 2008. Mathematical models for somite formation. Curr. Top. Dev. Biol., 183–203.

Cooke, J., Zeeman, E. C., 1976. A clock and wavefront model for control of the number of repeated structures during animal morphogenesis. J. Theor. Biol. 58 (2), 455.

Dequéant, M. L., Glynn, E., Gaudenz, K., Wahl, M., Chen, J., Mushegian, A., Pourquié, O., 2006. A complex oscillating network of signaling genes underlies the mouse segmentation clock. Science 314 (5805), 1595–1598.

Dequéant, M. L., Pourquié, O., 2008. Segmental patterning of the vertebrate embryonic axis. Nat. Rev. Gen. 9 (5), 370–382.

Dubrulle, J., McGrew, M. J., Pourquié, O., 2001. FGF signaling controls somite boundary position and regulates segmentation clock control of spatiotemporal Hox gene activation. Cell 106 (2), 219–232.

Gibb, S., Zagorska, A., Melton, K., Tenin, G., Vacca, I., Trainor, P., Maroto, M., Dale, J. K., 2009. Interfering with Wnt signalling alters the periodicity of the segmentation clock. Dev. Biol. 330 (1), 21–31.

Gilbert, S. F., 1997. Developmental Biology, 5th Edition. Sinauer Associates.

Giudicelli, F., Özbudak, E. M., Wright, G. J., Lewis, J., 2007. Setting the tempo in development: an investigation of the zebrafish somite clock mechanism. PLoS Biol. 5 (6), e150.

Gomez, C., Özbudak, E. M., Wunderlich, J., Baumann, D., Lewis, J., Pourquié, O., 2008. Control of segment number in vertebrate embryos. Nature 454 (7202), 335–339.

Gomez, C., Pourquié, O., 2009. Developmental control of segment numbers in vertebrates. J. Exp. Zool. B (Mol. Dev. Evol.) 312 (6), 533–544.

Accepted manuscript

ACCEPTED MANUSCRIPT

Herrgen, L., Ares, S., Morelli, L. G., Schröter, C., Jülicher, F., Oates, A. C., 2010. Intercellular coupling regulates the period of the segmentation clock. Curr. Biol. 20.

Horikawa, K., Ishimatsu, K., Yoshimoto, E., Kondo, S., Takeda, H., 2006. Noise-resistant and synchronized oscillation of the segmentation clock. Nature 441 (7094), 719–723.

Jiang, Y. J., Aerne, B. L., Smithers, L., Haddon, C., Ish-Horowicz, D., Lewis, J., 2000. Notch signalling and the synchronization of the somite segmentation clock. Nature 408 (6811), 475–479.

Kuramoto, Y., 1981. Rhythms and turbulence in populations of chemical oscillators. Physica A 106 (1-2), 128–143.

Lewis, J., 2003. Autoinhibition with transcriptional delay: A simple mechanism for the zebrafish somitogenesis oscillator. Curr. Biol. 13 (16), 1398–1408.

Monk, N. A. M., 2003. Oscillatory expression of Hes1, p53, and NF-κB driven by transcriptional time delays. Curr. Biol. 13 (16), 1409–1413.

Morelli, L. G., Ares, S., Herrgen, L., Schröter, C., Jülicher, F., Oates, A. C., 2009. Delayed coupling theory of vertebrate segmentation. HFSP J. 1 (3), 55–66.

Murray, J. D., 1989. Mathematical Biology, 3rd Edition. Springer.

Ockendon, J. R., Howison, S., Lacey, A., Movchan, A., 2003. Applied Partial Differential Equations. Oxford University Press.

Özbudak, E. M. and Lewis, J., 2008. Notch signalling synchronizes the zebrafish segmentation clock but is not needed to create somite boundaries. PLoS Genet. 4 (2), e15.

Riedel-Kruse, I. H., Muller, C., Oates, A. C., 2007. Synchrony dynamics during initiation, failure, and rescue of the segmentation clock. Science 317 (5846), 1911.

Schröter, C., Herrgen, L., Cardona, A., Brouhard, G. J., Feldman, B., Oates, A. C., 2008. Dynamics of zebrafish somitogenesis. Dev. Dyn. 237 (3), 545.

Schröter, C., Oates, A. C., 2010. Segment number and axial identity in a segmentation clock period mutant. Curr. Biol. 20.

Tiedemann, H. B., Schneltzer, E., Zeiser, S., Rubio-Aliaga, I., Wurst, W., Beckers, J., Przemeck, G. K. H., Hrabé de Angelis, M., 2007. Cell-based simulation of dynamic expression patterns in the presomitic mesoderm. J. Theor. Biol. 248 (1), 120–129.

Uriu, K., Morishita, Y., Iwasa, Y., 2010. Random cell movement promotes synchronization of the segmentation clock. Proc. Nat. Acad. Sci. 107 (11), 4979.

Whitham, G. B., 1974. Linear and Nonlinear Waves. New York, Wiley-Interscience.

Accepted manuscript

ACCEPTED MANUSCRIPT

A. Deriving the continuum model

A.1. A molecular model of coupled oscillators

In order to demonstrate how a chain of underlying oscillators can lead to the phase equation (1), we consider a chain of $\lambda - \omega$ oscillators with the uncoupled dynamics of the k^{th} oscillator given by

$$\begin{aligned} \dot{u}_k &= \omega v_k + P u_k(1 - u_k^2 - v_k^2), \\ \dot{v}_k &= -\omega u_k + P v_k(1 - u_k^2 - v_k^2); \end{aligned} \tag{37}$$

where the parameter ω is the oscillation frequency and the parameter P represents the strength of attraction of the limit cycle. Making the coordinate transformation

$$\begin{aligned} u_k &= r_k \cos\theta_k, \\ v_k &= r_k \sin\theta_k; \end{aligned} \tag{38}$$

equations (37) transform to

$$\begin{aligned} \dot{r}_k &= P r_k(1 - r_k), \\ \dot{\theta}_k &= \omega; \end{aligned} \tag{39}$$

which have long time periodic solution

$$\dot{\theta}_k = \omega, \tag{40}$$

$$r_k = 1. \tag{41}$$

Introducing linear and quadratic coupling terms, of strengths A and B, respectively, into equations (37), we obtain

$$\begin{aligned} \dot{u}_k &= \omega v_k + P u_k(1 - u_k^2 - v_k^2) + \tilde{A}\left(u_{k-1} - 2u_k + u_{k+1}\right) - \tilde{B} v_k\left((u_{k+1} - u_k)^2 + (v_{k-1} - v_k)^2\right); \\ \dot{v}_k &= -\omega u_k + P v_k(1 - u_k^2 - v_k^2) + \tilde{A}\left(v_{k-1} - 2v_k + v_{k+1}\right) - \tilde{B} u_k\left((u_{k+1} - u_k)^2 + (v_{k-1} - v_k)^2\right), \end{aligned} \tag{42}$$

Making the coordinate transformation (38) and considering the system in the limit of $P \gg \tilde{A}$, this model transforms to a discretised version of equation (1):

$$\frac{d\theta_k}{dt} = \omega + \tilde{A}\left(\theta_{k-1} - 2\theta_k + \theta_{k+1}\right) - \frac{\tilde{B}}{2}\left((\theta_k - \theta_{k-1})^2 + (\theta_k - \theta_{k+1})^2\right). \tag{43}$$

The radial dynamics are approximately

$$r_k \sim 1. \tag{44}$$

Equation (43) describes how the phase of the k^{th} oscillator is updated as a result of interactions with its nearest neighbours. In order to take the continuum limit of this system we assume that the coupling parameters $\tilde{A}$ and $\tilde{B}$ scale with the variable $1/(\Delta k)^2$ such that

$$A = \tilde{A}\Delta k^2; \qquad B = \tilde{B}\Delta k^2. \tag{45}$$

Accepted manuscript

ACCEPTED MANUSCRIPT

Thus equation (43) can be written in the form

$$\frac{d\theta_k}{dt} = \omega + A\left(\frac{\theta_{k-\Delta k} - 2\theta_k + \theta_{k+\Delta k}}{\Delta k^2}\right) - \frac{B}{2}\left(\left(\frac{\theta_k - \theta_{k-\Delta k}}{\Delta k}\right)^2 + \left(\frac{\theta_k - \theta_{k+\Delta k}}{\Delta k}\right)^2\right). \tag{46}$$

We assume that the limit

$$\lim_{\Delta k \to 0} \frac{\theta_{k+1} - \theta_k}{\Delta k} \tag{47}$$

exists and is well defined, and define the partial derivative

$$\frac{\partial \theta}{\partial k} = \lim_{\Delta k \to 0} \frac{\theta_{k+1} - \theta_k}{\Delta k}, \tag{48}$$

such that unit length is related to oscillator index via the relationship

$$\Delta k = d\Delta x, \tag{49}$$

where the parameter d represents one cell diameter. Hence the discrete equation (46) transforms to the continuum equation (1). As oscillator phase is defined modulo 2π we place a further restriction on the validity of the model:

$$\frac{\partial \theta}{\partial k} < \pi. \tag{50}$$

The continuum model can only be a valid description of oscillator dynamics so long as neighbouring oscillators are separated in phase by no more than π.

B. A phase description of a system of coupled oscillators in one spatial dimension

B.1. The limit of the discrete phase model

Consider a 1D chain of identical oscillators with the phase dynamics of the i^{th} oscillator given by the ODE

$$\frac{d\theta_k}{dt} = \omega + \sum_j (A\sin(\theta_j - \theta_k) + B(\cos(\theta_j - \theta_k)) - 1), \tag{51}$$

where ω is the angular frequency and A and B are coupling strength parameters (which we assume to be positive). Making the approximation that neighbouring oscillators are close together in phase such that

$$|\theta_k - \theta_{k-1}| \ll 1; \tag{52}$$

$$|\theta_k - \theta_{k+1}| \ll 1; \tag{53}$$

then expanding out the cos and sin terms in equation (51) yields

$$\frac{d\theta_k}{dt} = \omega + A(\theta_{k-1} - 2\theta_k + \theta_{k+1}) + B\left(1 - \frac{(\theta_{k-1} - \theta_k)^2}{2} + ... + 1 - \frac{(\theta_{k+1} - \theta_k)^2}{2} + ...\right) - 2B, \tag{54}$$

$$= \omega + A(\theta_{k-1} - 2\theta_k + \theta_{k+1}) - \frac{B}{2}\left((\theta_{k-1} - \theta_k)^2 + (\theta_{k+1} - \theta_k)^2\right) + O(\Delta\theta^3). \tag{55}$$

Accepted manuscript

ACCEPTED MANUSCRIPT

Now assuming that the coupling strengths A and B scale such that $A = \hat{A}/\Delta k^2$ and $B = \hat{B}/\Delta k^2$ we obtain

$$\frac{d\theta_k}{dt} = \omega + \hat{A}\frac{(\theta_{k-1} - 2\theta_k + \theta_{k+1})}{\Delta k^2} - \frac{\hat{B}}{2\Delta k^2}\left((\theta_{k-1} - \theta_k)^2 + \theta_{k+1} - \theta_k)^2\right) + O(\Delta\theta^3). \tag{56}$$

Making the assumption that a finite difference approximation of first order derivatives is given by

$$\frac{\partial\theta}{\partial k} \sim \frac{\theta_{k+1} - \theta_k}{\Delta k}, \tag{57}$$

or

$$\frac{\partial\theta}{\partial k} \sim \frac{\theta_k - \theta_{k-1}}{\Delta k}, \tag{58}$$

then taking the continuum limit of equation (56) for $1 \ll \Delta k \ll N$ gives

$$\frac{\partial\theta}{\partial t} = \omega + \hat{A}\frac{\partial^2\theta}{\partial k^2} - \frac{\hat{B}}{2}\left(\left(\frac{\partial\theta}{\partial k}\right)^2 + \left(\frac{\partial\theta}{\partial k}\right)^2\right) \tag{59}$$

$$= \omega + \hat{A}\frac{\partial^2\theta}{\partial k^2} - \hat{B}\frac{\partial\theta}{\partial k}^2. \tag{60}$$

Accepted manuscript

ACCEPTED MANUSCRIPT

We propose an alternative formulation of Cooke and Zeeman's clock and wavefront model.

The wavefront is a gradient in clock phase and an emergent model phenomenon.

The model is applied to zebrafish, snake, chick and mouse data.

The model exhibits excellent agreement with experimental data.

Observed perturbations associated with transplant experiments are reproduced.

Accepted manuscript